Materials Science & Engineering A 943 (2025) 148858

Contents lists available at ScienceDirect

Materials Science & Engineering A

journal homepage: www.elsevier.com/locate/msea

Structure-property correlation in multi-phase steels by correlative electron back scattered diffraction and nanoindentation mapping

S. Janakiram [a], Harita Seekala [b], Chavan Akash Naik [a], S. Chen [c], J.W.H. van Krevel [c], Leo A.I. Kestens [d,e], J. Gautam [a,*], P. Sudharshan Phani [a,**]

[a] School of Engineering Sciences and Technology, University of Hyderabad, India
[b] International Advanced Research Centre for Powder Metallurgy and New Materials (ARCI), Hyderabad, India
[c] Tata Steel R&D, PO Box 10000, IJmuiden, 1970 CA, the Netherlands
[d] Department of Electromechanics, Systems and Metals Engineering, Ghent University, Ghent, Belgium
[e] Materials Science and Engineering Department, Delft University of Technology, 2628 CD, Delft, the Netherlands

ARTICLE INFO

Keywords:
Microstructural characterization
Multiphase microstructure
TRIP
DH steels
Micro-macroscale property
Correlative microscopy

ABSTRACT

The current study investigates the microscale mechanical properties of the constituent phases and their influence on the macroscale properties of multi-phase steels with different microstructural constituents. Two steels, a Transformation Induced Plasticity (TRIP) and an enhanced ductility Dual Phase (DH) steel were produced in a continuous annealing line (CAL). Optical microscopy and EBSD results were utilized for segmentation of microstructural phase constituents. Macroscale mechanical properties were obtained using tensile testing and microscale properties with nanoindentation mapping. The hardness of each constituent is extracted from the hardness maps using a clustering algorithm. TRIP steel shows a homogeneous distribution of retained austenite in ferrite matrix and a small amount of bainite/martensite which is non-banded. In contrast, DH steel shows heterogeneous microstructures where martensite/bainite/retained austenite is found to be banded in the ferrite matrix. Both steels exhibit notable variations in hardness across their constituent phases, which are associated with the resulting microstructural characteristics. Nanoindentation results show that overall hardness/strength in TRIP steel is contributed from ferrite (66 %), retained austenite (33 %) and martensite/bainite (1 %). Whereas in DH steel, it is contributed from ferrite (55 %), mixture of RA, martensite/bainite (~40 %) and martensite (~5 %). The macroscopic behavior of TRIP and DH steels was explained and discussed using the rule of mixtures in conjunction with the microscopic properties of individual phases.

1. Introduction

Transformation induced plasticity (TRIP) and enhanced ductility/formability cold rolled DP steels (DH grades) are classified as *third generation advanced high strength steels* (3G AHSS) with good combination of strength and high ductility and are mainly utilized in automotive parts [1–4]. TRIP and DH steel sheets are typically produced in continuous galvanizing lines (CGL), where the cold rolled steels undergo a two-stage process: intercritical annealing (IA) and austempering around 350–460 °C for isothermal bainite transformation (IBT) [2,5,6]. During IA, partial formation of austenite and partitioning of alloying elements take place [7], while during austempering the formation of bainite and partitioning of carbon take place to enrich the remaining austenite [8–10]. This two-stage processing leads to the development of the heterogeneous multiphase microstructures of hard martensite/-bainite and retained austenite, embedded in a ductile ferrite matrix. The morphology and phase fractions depend on the steel chemical composition, hot band microstructure and the annealing process parameters [2,11]. In general, ferrite facilitates ductility, while bainite/martensite enhances strength and retained austenite enhances both strength-ductility [12]. The multiphase microstructure is inherently heterogeneous (with variations in local features such as phase/precipitate size and shape, grain orientations, grain/phase boundaries, dislocation densities) [13,14]. It is well known that, along with the

This article is part of a special issue entitled: Nanomechanical Testing 2024 published in Materials Science & Engineering A.

* Corresponding author.
** Corresponding author.
E-mail addresses: jaiprakashgautam@uohyd.ac.in (J. Gautam), spphani@uohyd.ac.in (P.S. Phani).

https://doi.org/10.1016/j.msea.2025.148858
Received 3 April 2025; Received in revised form 18 July 2025; Accepted 21 July 2025
Available online 22 July 2025

microstructure, the constituent phase properties play a crucial role in determining the overall deformation/mechanical behaviors of AHSS [15–17]. Therefore, accurate characterization of the constituent phase properties and their influence on overall macro scale deformation behavior is important in the study of AHSS.

Recently, nanoindentation mapping method has been applied to estimate the constituent phase properties during recovery and partial recrystallization and phase transformation of a AHSS [18–20]. This technique shows advantages over other methods for the study of multiphase steels with micrometer microstructural features, with high-resolution, phase/grain-resolved hardness data. By combining energy dispersive spectroscopy (EDS), electron backscattered diffraction (EBSD), electron probe microanalysis (EPMA), with automated nanoindentation, previous studies have successfully correlated the compositional variation and microstructural characteristics with local hardness [21–23]. However, the influence of these local phase-specific properties on the overall macroscale deformation and mechanical behavior has not been fully established. Specifically, Chang et al. [24] investigated the influence of compositional heterogeneity, on the microscopic mechanical properties in DP800 and CP800 multiphase steels with nanoindentation mapping. While the fundamental principles of microstructure–property relations in TRIP and DH steels are well established [2,4,25,26], the microscale response of each individual phase and its relative quantitative contribution to the macroscopic flow/deformation behavior has not been well studied. The presence of retained austenite in these steels further adds complexity by TRIP effect that requires local analysis.

To address this gap, the present study provides new quantitative evidence by directly linking local phase-specific mechanical properties and phase fractions — mapped at high spatial resolution by correlative EBSD–nanoindentation — with bulk macroscale tensile behavior. The rule of mixtures technique, together with microscopic properties of individual phases, was utilized to explain macroscopic behavior in two different microstructural constituents of TRIP and DH steels. The finding of this study increase the knowledge on heterogeneity of multiphase steels and its impact on the local mechanical property which could help optimize the process and performance of steels in a variety of industrial applications. In addition, it helps bridging the gap between small scale features (like grain structure, phase distribution and dislocation behavior) and the macro scale properties (like strength, local and global ductility).

2. Materials and methods

2.1. Materials

The materials used in the work were provided by TATA Steel Netherlands IJmuiden. The chemical compositions of the TRIP and DH steels are shown in Table 1. TRIP and DH steel sheets of 1.2 mm or 1.4 mm thick were produced by continuous annealing. The actual temperature and time of the heat treatments are not provided due to confidentiality. The material utilized here, however, is merely intended to illustrate how correlative characterization using nanoindentation and EBSD aids in determining the microscopic properties of different phases in multiphase AHSS which can be further used to explain the macroscopic behavior. Using Kasatkin formulas [25], the Ac1 and Ac3 temperatures representing the start and finish of austenite formation during heating of the steels were calculated and reported in Table 1.

Table 1
Chemical composition of TRIP and DH steels (in wt.%).

Sample	C	Mn	Si + Al	Cr	Ni	Nb + Ti + V	Ac1 [°C]	Ac3 [°C]
TRIP	0.214	1.18	1.8	0.04	0.0068	0.0066	727	950
DH	0.142	1.82	1	0.43	0.0253	0.0119	723	865

2.2. Microstructural characterization

The microstructural observations and nanoindentation measurements were performed on the cross section of the rolling and normal direction (RD-ND plane) of the steel sheets. Samples were mechanically polished. Final vibratory polishing was performed using colloidal silica of 50 nm for 10 h. Light optical microscopy (LOM) was carried out using an Olympus (GX51 model) type instrument. Color tint etching was first performed using Nital followed by $Na_2S_2O_5$ + water for tinting. This etching has been shown to reveal ferrite with light brown contrast, brown to dark brown for martensite/bainite and off-white for retained austenite in TRIP steels reported in a previous work [27]. The micro constituents in the multi-phase microstructures were identified by image analysis using open source trainable WEKA segmentation of FIJI plugin (ImageJ) [28,29].

Scanning electron micrographs were obtained using a FE-SEM (FEI NOVA NANOSEM 450 model) with an accelerating voltage of 20 kV and a working distance of 15 mm. EBSD mapping was performed using the velocity detector by TSL-EDAX at a step size of 80 nm. Post processing analysis of EBSD data were performed using TSL-OIM software version 8.6. The data set obtained from the EBSD map was used to identify FCC and BCC phase. In the BCC phase, ferrite and martensite were distinguished based on image quality (IQ) of the diffraction pattern as reported in Ref. [30]. Kernel average misorientation (KAM), calculated with the 5th nearest neighbor and a tolerance limit of 3° misorientation, was used to measure the local misorientation.

2.3. Mechanical testing

Samples for tensile testing were prepared using ASTM -E8/E8M standards (length = 50 mm; width = 7 mm), with rolling direction parallel to the tensile axis. Room temperature tensile tests were performed using an Instron 5982 universal servo-hydraulic testing system to determine yield strength (YS), ultimate tensile strength (TS), total elongation (TE) and uniform elongation (UE) were determined. Yield strength values were obtained using the conventional 0.2 % stain offset. Three specimens were tested for each condition. The average with standard deviations was reported.

The well-polished samples were subjected to nanoindentation tests. A commercially available iMicro® nanoindenter from Nanomechanics Inc. (now KLA Corporation), Oak Ridge, USA, equipped with an InForce50 actuator was used for nanoindentation mapping. All measurements were performed using a diamond Berkovich tip (E = 1141 GPa, v = 0.07). At least 4 indentation maps with 2500 indents per map for each sample covering a 50 μm by 50 μm area were collected using the NanoBlitz3D high-speed mapping approach. Based on the recommendation of the previous work of Phani et al. [31], a load that would produce an indentation depth of 100 nm or less was chosen while maintaining an indentation spacing of 1 μm in order to maintain a minimal spacing to depth ratio of 10. Following these recommendations, the chosen 1 μm indent spacing ensures minimal effect of neighboring indents.

3. Results

3.1. Microstructural evolution by light optical microscopy

Optical micrographs of TRIP and DH steels are shown in Fig. 1. The microstructure consists of polygonal ferrite (light brown), bainite/martensite (brown and dark brown) and retained austenite (white), as shown in Fig. 1(a and c). In the corresponding segmented images as shown in Fig. 1 (b and d), the polygonal ferrite appears blue, bainite/martensite in red and austenite in off-white. The quantification of segmented micro constituents using WEKA plugin are summarized and

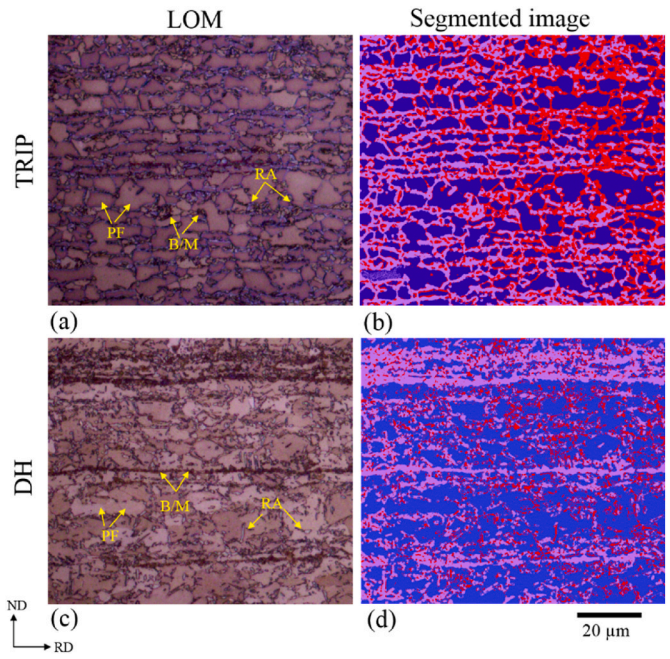

Fig. 1. Optical micrograph and segmented image of (a–b) TRIP and (c–d) DH steel in RD-ND plane. Etched using Nital/$Na_2S_2O_5$, retained austenite (off-white), martensite/bainite (brown/dark brown), ferrite (light brown), corresponding segmented image shows ferrite (blue), bainite/martensite (grey) and retained austenite (red).

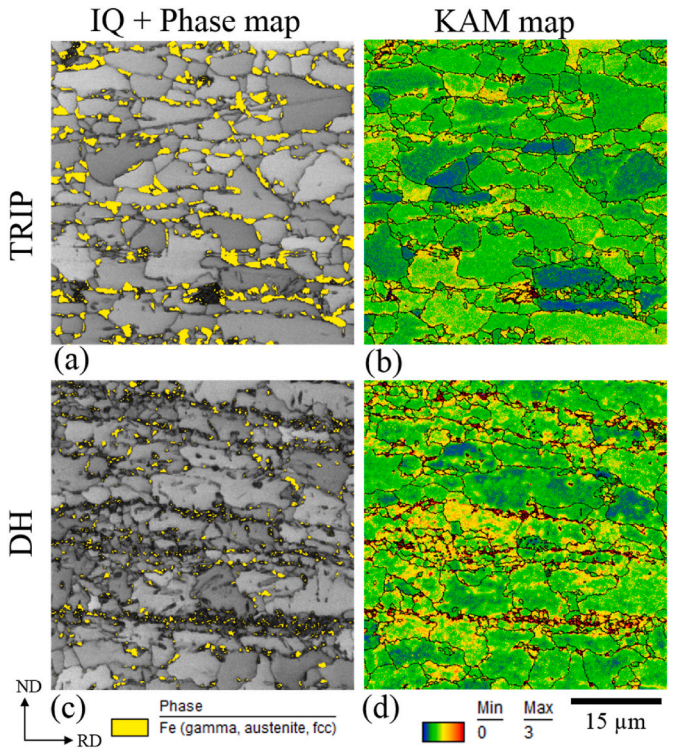

Fig. 2. IQ + phase map and corresponding KAM map in RD-ND plane of (a–b) TRIP and (c–d) DH steels.

listed in Table 2. It clearly shows the lower ferrite, retained austenite contents and higher bainite/martensite in DH steel compared to TRIP steel. TRIP steel shows a more homogenous microstructure, whereas DH steel is featured by a heterogeneous microstructure with micro-segregation bands of bainite/martensite. The differences in distribution of bainite/martensite between TRIP and DH steels can be linked to the differences in the steel chemistry particularly Mn content which causes banding [33].

3.2. Microstructural evolution by EBSD

Fig. 2 shows the EBSD micrographs of the two steels. In the combined image quality (IQ) and phase map of RA (Fig. 2(a) and c), the BCC phase is shown in grey and the FCC phase (retained austenite) in yellow. It can clearly be observed that RA grains are of smaller size. The IQ and KAM maps were used to distinguish martensite from ferrite in the BCC phase. Martensite, with larger lattice distortions due to increased dislocation density, density of subgrain boundaries, displays a diffused diffraction contrast on the IQ map, as seen in Fig. 2(a) and (c). The corresponding KAM maps in Fig. 2(b) and (d) show higher KAM values in areas with lower IQ, indicating more lattice deformation in martensite. The areas with a lower KAM value and higher IQ correspond to ferrite. Martensite and ferrite were distinguished using a combination of IQ and KAM (measured for the 5th nearest neighbor with a 3° misorientation). In the TRIP steel, the retained austenite appears coarse, with blocky (γB) and filmy (γF) morphologies along the grain boundaries. In DH steel, it is much finer, with blocky (γB) morphology present both inside and along the ferrite grain boundaries. Table 3 shows the quantification of the BCC and FCC phases, with TRIP steel having a higher fraction of retained austenite compared to DH steel.

Table 2
Micro constituent quantification from LOM images for TRIP and DH steels.

Sample	Ferrite [%]	B/M [%]	RA [%]
TRIP	79 ± 4.3	9 ± 4.6	12 ± 2.8
DH	67 ± 5.8	27.5 ± 5.3	5.5 ± 2.1

Table 3
Micro constituent's quantification from EBSD for TRIP and DH steels.

Sample	BCC	FCC	Grain size BCC [μm]	Grain size RA [μm]
TRIP	90.2 ± 4.3	9.8 ± 2.1	6.5 ± 3.1	0.84 ± 0.3
DH	96.7 ± 5.8	3.3 ± 1.3	5.9 ± 3.5	0.41 ± 0.2

TRIP steel contains small isolated dispersed blocky martensite, whereas DH steel exhibits more extensive martensite regions that appear continuous along bands. KAM maps show higher KAM values in martensite and lower values in ferrite. Intermediate KAM values are observed in ferrite close to ferrite/martensite interfaces, as shown in Fig. 2(c) and (d). The distribution of KAM values is relatively heterogeneous around martensite and regions affected by martensite, as seen in Fig. 2(d). Additionally, higher KAM values are observed in localized areas inside ferrite, in small grains, and along ferrite-ferrite boundaries, though these are less frequent and less pronounced compared to ferrite/martensite interfaces [34,35].

In summary, DH steel, which exhibits a higher martensite content, shows higher KAM values in ferrite near the ferrite/martensite interfaces compared to TRIP steel with less martensite. The KAM value distribution within ferrite grains is quite heterogeneous for both steels.

3.3. Tensile testing

The engineering stress-strain curves in Fig. 3 show the macroscopic response of TRIP and DH steels. The mechanical properties are shown in Table 4. TRIP steel shows a lower yield strength, tensile strength and a higher elongation compared to DH steel. TRIP steel shows yield point phenomena and discontinuous yielding, whereas DH steel shows continuous yielding.

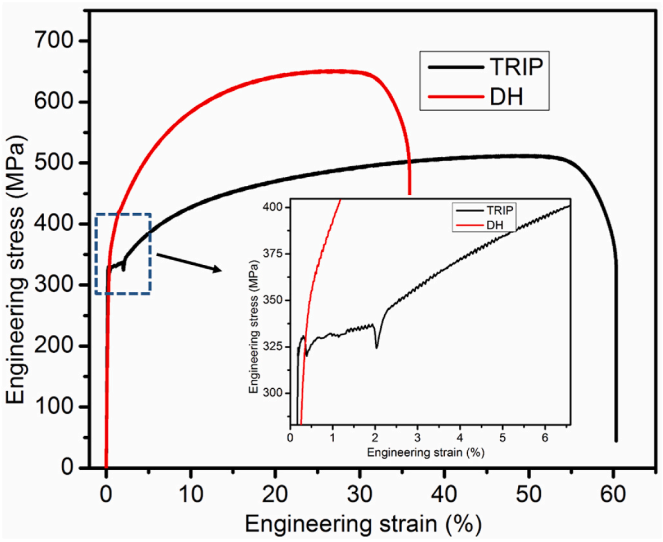

Fig. 3. Engineering stress strain curve of TRIP and DH steels.

Table 4
Macroscopic mechanical properties of TRIP and DH steels.

Sample	Yield strength [MPa]	Tensile strength [MPa]	Total Elongation [%]	Hardness [GPa]
TRIP	320 + 12.86	512 + 14.75	60.3 + 1.21	3.7 ± 1.09
DH	366 ± 15.56	660 ± 13.78	35.9 ± 0.05	4.4 ± 1.77

3.4. Nanoindentation mapping

To measure hardness at the length scale of the individual phases high speed-high resolution nanoindentation mapping is performed. In Fig. 4, we show IQ map and corresponding nanoindentation hardness map on both TRIP and DH steels. The average hardness for the entire map is reported in Table 4. In the IQ map shown in Fig. 4 (a and c), the higher IQ (grey) domains correspond to ferrite, whereas the lower IQ (dark grey) regions represent bainite/martensite and retained austenite.

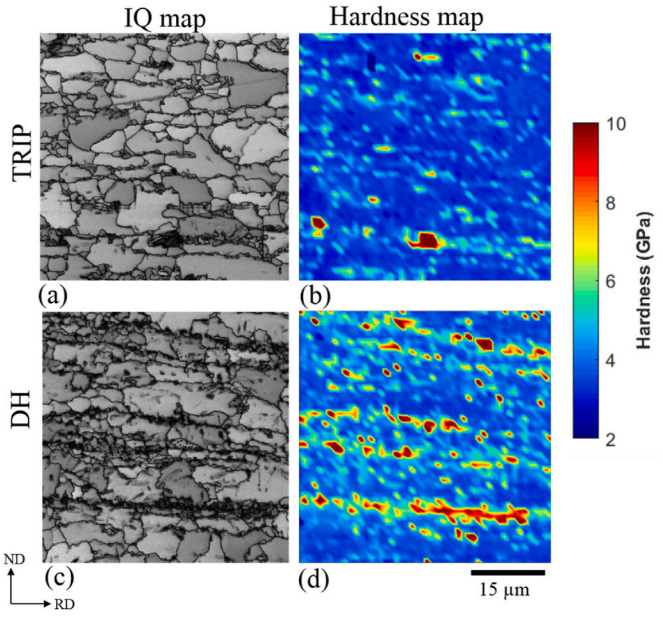

Fig. 4. IQ map and corresponding hardness map in (a–b) TRIP and (c-d) DH steel.

Excellent correlation between the IQ map and the hardness map can be observed with the high IQ regions corresponding to ferrite showing lower hardness (2–4 GPa) and the low IQ regions (RA/bainite/martensite) showing higher hardness (4–10 GPa). A closer comparison of the IQ and hardness maps shows that the hardness of DH steel is higher than that of TRIP steel, similar to the macroscopic results shown in Table 4. The deconvoluted hardness of the individual constituents and the one-to-one correlation with microstructure will be presented in the next section.

4. Discussion

In this section the microscale mechanical properties of individual phase constituents is analyzed to explain the macroscale response, which forms the basis for structure property correlation in TRIP and DH steels.

4.1. Deconvolution of microscale mechanical properties

The hardness maps are deconvoluted and compared to microstructural phase features in order to objectively examine the hardness of individual phases in the microstructure, cf. Fig. 5. The phase map obtained from EBSD displays martensite (red), retained austenite (yellow), and ferrite (grey) as shown in Fig. 5(a). Distinct hardness differences are observed in the corresponding hardness map of a similar location in Fig. 5(b) and exhibits a strong correlation with the phase map derived by EBSD. Hardness map was deconvoluted using K-means clustering algorithm as reported in Refs. [18,20,32]. Three mechanically distinct hardness regions in blue, cyan and red color were observed from the deconvolution phase map as shown in Fig. 5(c). The highest hardness areas correspond to martensite, which is red in color, and the lowest hardness corresponds to ferrite, which is blue in color. In TRIP steel, the deconvoluted map's cyan color correlates with the mixed phase region, which is primarily composed of retained austenite (yellow) as well as epitaxial ferrite/bainite and grain boundaries. In DH steel, the cyan color mixed region consists of retained austenite, epitaxial ferrite, bainite, and small martensite phases. It may be noted that the exact estimation of hardness in retained austenite, bainite, epitaxial ferrite or fine martensite colonies on grain boundaries is challenging due to its finer length scales. Overall, an excellent correlation exists between the microstructural phase features, hardness map and deconvoluted map in Fig. 5. The hardness of individual phase features is shown in Table 5. In TRIP steel, ferrite has the lowest hardness (3.3 ± 0.23 GPa), the mixed phase region that is comprised of one or more of retained austenite, bainite/fine martensite and epitaxial ferrite has an intermediate hardness (4.9 ± 1 GPa), and martensite has the highest hardness (11.6 ± 1.6 GPa). In DH steel, ferrite has the lowest hardness (3.7 ± 0.32 GPa), followed by the mixed phase region (5.7 ± 1.2 GPa), and martensite (10.8 ± 1.2 GPa) at the maximum.

4.2. Rationalization of macroscale properties through small scale testing

The microscale mechanical properties obtained from nanoindentation mapping are now used to explain the macroscopic behavior of TRIP and DH. By combining microstructural data with the microscopic properties obtained from Fig. 5 and Table 5, we apply the rule of mixtures to rationalize how these local characteristics contribute to the overall macroscopic strength, as shown in Fig. 6. Mainly two aspects will be discussed: changes in the yield/tensile strength and elongation. The average hardness from rule of mixtures is calculated by the weighted average of the hardness of each of the constituents, with weight factors equal to the area fraction of these constituents. Using such a rule of mixtures, it can be shown that the overall hardness in TRIP steel at a 512 MPa level has a major contribution of 66 % from ferrite, 33 % from mix region which is predominantly retained austenite and ~1 % from bainite/martensite, cf. Fig. 6. In a DH steel at a strength level of around

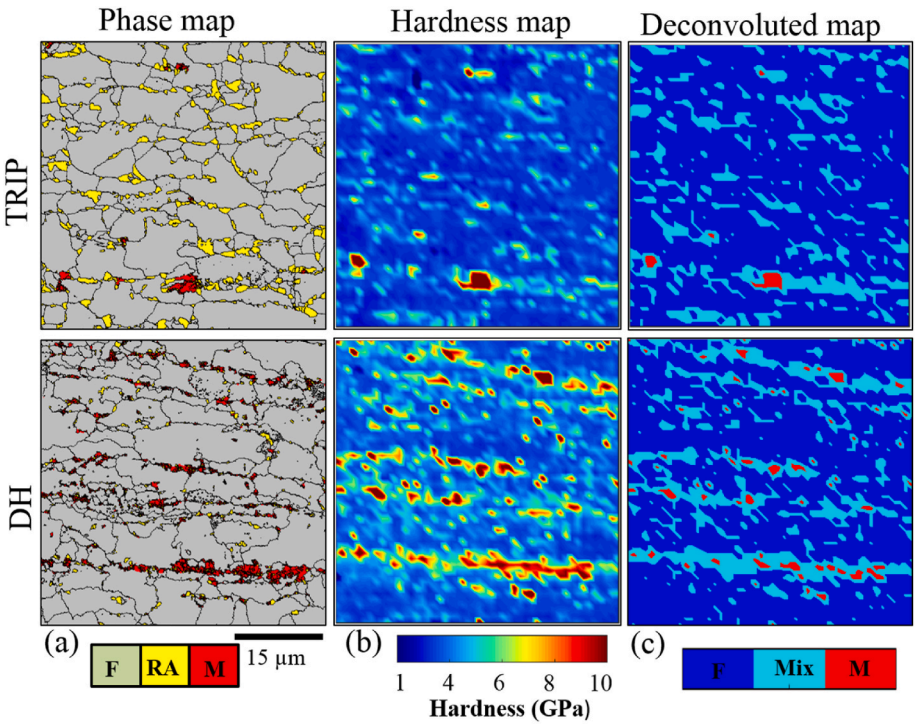

Fig. 5. (a) Phase map obtained from EBSD and the corresponding (b) hardness map and (c) deconvoluted hardness map for TRIP and DH steels.

Table 5
Comparison of microscale mechanical properties (Hardness) of individual phases in TRIP and DH steels.

Sample	**Ferrite (F)**	Mix phase	**Martensite (M)**	**Ferrite (F)**	Mix phase	**Martensite (M)**
	Hardness (GPa)			Area fraction (%)		
TRIP	3.3 ± 0.23	4.9 ± 1	11.6 ± 1.6	74.2	25.16	0.68
DH	3.7 ± 0.32	5.7 ± 1.2	10.8 ± 1.2	65.6	30.28	4.12

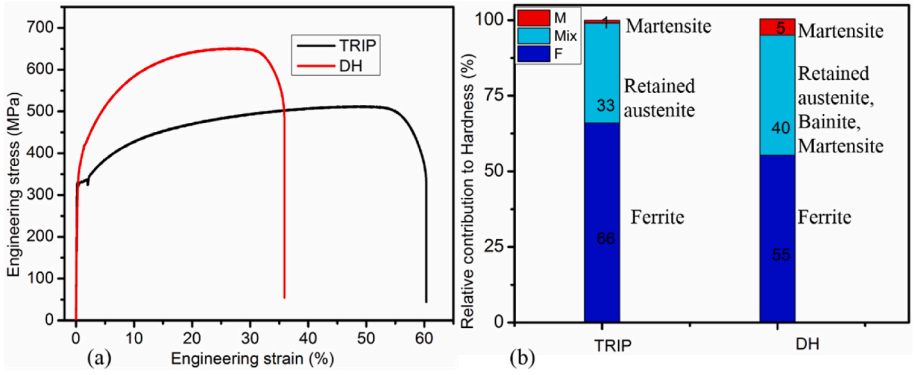

Fig. 6. Contribution of individual phase hardness to overall hardness or strength in TRIP and DH steels.

660 MPa, ferrite contributes about 55 %, mixed region (retained austenite/bainite/fine martensite/epitaxial ferrite) contributes 40 % and martensite contributes 5 %. These results show that for these grades, a higher fraction of secondary phase constituents and their properties contribute to the overall higher tensile strength in the DH steel (660 MPa) compared to TRIP steel (512 MPa).

The yield strength of DH steel (366 MPa) was slightly higher than that of TRIP steel (320 MPa), and yielding was continuous in DH and discontinuous in TRIP, as shown in Fig. 3. The different yield behavior can be linked to the differences in microstructural phase constituents and their interaction. Fig. 6(b) shows that hard phases (mix and martensite) contribute about 45 % to the strength in DH steel, whereas it is about 1 % in TRIP, as retained austenite does not contribute so much to hardening as martensite. This in turn is due to a higher content of bainite/martensite micro segregation bands in DH steel. During the last cooling continuous annealing step, Geometrically Necessary Dislocations (GNDs) form due to accommodation of the volume and shape change that is associated with the transformation from austenite to hard martensite [36]. As this accommodation partially occurs by plastic deformation, it generates a high density of mobile dislocations, leading

to continuous yielding of DH steel [36] at the elastic limit. The higher martensite/bainite content, interacting with the lower ferrite content, generates larger residual compressive stresses contributing to the strength [37]. Higher concentrations of Si and precipitate-forming elements such as Cr, Ti, V, and Nb, also present in DH steel, cause precipitation hardening [38,39].

Conversely, in the case of TRIP steel, as shown in Fig. 6(b), the contribution of secondary phase constituents such as martensite/bainite is less than 1 %. Strength is obtained from the ductile retained austenite and ferrite which results in lower yield strength. IQ and KAM maps in Fig. 2(a and b) show a fine dispersed distribution of bainite/martensite and retained austenite which does not generate a high GND density. This leads to lower yield strength and discontinuous yielding. Additionally, carbon dissolved in ferrite after IA might immobilize the dislocation generated during cooling to IBT and contributes to discontinuous yielding [40–42].

Local ductility is enhanced by minimizing local hardness differences in addition to UTS. The difference in hardness (ΔH) between the soft ferrite matrix and the other hard phases is shown in Fig. 7. It is observed that the difference in hardness is higher in DH than in TRIP. The differences in the hardness and elongation in TRIP and DH can be linked to the differences in the microstructure as shown in Figs. 1–4. The mixed region primarily consists of retained austenite in TRIP, and it consists of a mixture of epitaxial ferrite/retained austenite/bainite/martensite in DH steel as shown in Fig. 5. It may be noted that retained austenite contributes about 33 % to hardness in the case of TRIP. The hardness difference between relatively softer retained austenite and soft ferrite matrix will be thereby smaller in the case of TRIP as shown in Fig. 7 and together with the TRIP effect results in higher ductility. The hardness contribution in DH steel from the soft phase accounts for about 55 % and the contribution from the hard phases for about 45 %, resulting in a decrease in ductility. Hence, the differences mentioned above in microstructure, strength level and their local property causes higher hardness differences in DH steel compared to TRIP and also a lower elongation.

The microstructure of DH steel shows bainite/martensite microsegregation bands inherited from the casting due to a higher Mn contents. The alternation of hard martensite/bainite bands and soft ferrite bands leads to strain localization and this is shown in the KAM map of Fig. 2. These aspects cause hardness variations as shown in Fig. 4. The chemical heterogeneity and gradient in hardness as shown in Figs. 4 and 6(b) is detrimental to local formability as reported earlier [24]. Since

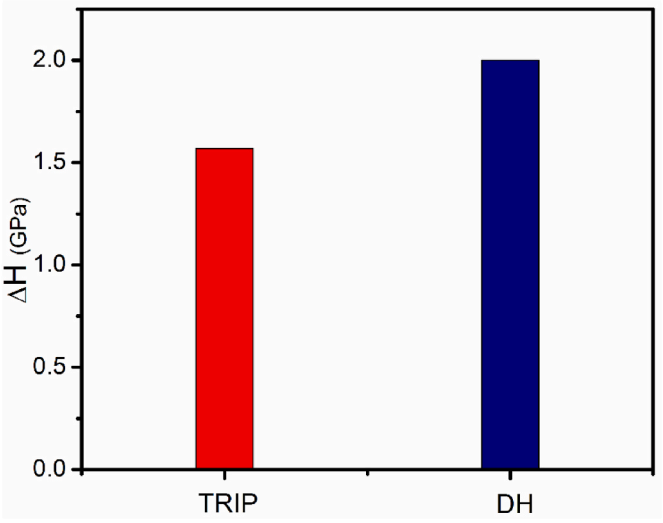

Fig. 7. Difference in hardness of secondary phase constituents and primary ferrite phase. The secondary phase is dominated by RA in TRIP and mixture of M, B, RA in DH steel.

there is less retained austenite in DH steel and more contribution of martensite/bainite to the strength, the microstructure is stiffer and less able to accommodate large plastic strains. As a result, DH steel has a higher strength, but a lower elongation compared to TRIP steel. Additionally, the reduced elongation of DH steel is due to the less potential for work hardening. Because of the TRIP effect, TRIP steel exhibits much better work hardening characteristics, which is responsible for the delay in the plastic instability that causes necking, strain localization and fracture.

The microstructure of TRIP steel revealed a more homogeneous distribution of ferrite, retained austenite and martensite/bainite as shown in Figs. 1 and 2. The hardness map in Fig. 4, shows a smooth transition of hardness gradient from ferrite to retained austenite and martensite, resulting in a beneficial effect on formability. Also TRIP steel has an increased Al content, which increases the two phase temperature window as shown in Table 1 and reported in Ref. [25] leading to homogeneous distribution of retained austenite and martensite/bainite in the ferrite matrix. TRIP steel consists of a small fraction of martensite and higher fraction of retained austenite as shown in Figs. 1, 2 and 6, whereby aluminum (Al) plays a key role in promoting carbon enrichment in retained austenite [26]. In this case, the carbon content in the retained austenite is around 1.5 wt%. This carbon enrichment enhances the stability of the retained austenite, delaying its transformation into martensite during deformation. As shown in Figs. 1 and 2, retained austenite with blocky and filmy morphology was seen, whereby filmy morphology is more observed in TRIP which is more stable. As a result, the stability of retained austenite contributes to improved ductility and less to strength in TRIP steels [9,22]. This stability effectively delays the transformation of austenite to martensite (TRIP effect), leading to higher elongation and improved local ductility, while maintaining adequate strength.

In this work, a quantitative link between local phase-specific mechanical properties and the bulk behavior of TRIP and DH steels has been established by showing a correlation between coupled EBSD-nanoindentation data at microscale and bulk tensile response. This approach can be extended to other similar alloy systems and processing conditions for the design and optimization of third-generation AHSS for lightweight automotive applications. While we have demonstrated the correlation for two different multiple phase steels, the framework provided in this work can be extended to other alloys/steels produced under different processing conditions to develop a comprehensive statistical model in the future.

While the present work applies K-means clustering to deconvolute phase-specific local mechanical data, the accuracy of phase classification could be further improved by incorporating supervised learning algorithms or semi-supervised approaches. These methods can be used to develop more robust correlations between EBSD-derived microstructural features and local mechanical properties.

5. Summary and conclusions

By coupling complementary techniques such as high-resolution nanoindentation mapping and electron microscopy (EBSD), microstructure-property correlations at the micrometer length scale were established for a TRIP steel and a DH multiphase steel to provide insights on contribution of microscopic properties on macroscopic behavior using small scale testing.

The following conclusions are drawn from the present work.

- The mechanical properties strongly depend on the microstructural phase features resulting from thermal treatments and chemical composition in both TRIP and DH steels.
- Nanoindentation results show that overall hardness (strength) in TRIP steel is contributed from ferrite (66 %), retained austenite (33 %) and martensite/bainite (1 %). Whereas in DH steel, overall

hardness/strength is contributed from ferrite (55 %), mixture of RA, martensite/bainite (~40 %) and martensite (~5 %).

- TRIP Steel is characterized by lower yield strength and high ductility/elongation compered to DH steel. The strength contribution is predominantly from soft ferrite (66 %) and retained austenite (33 %) leading to lower yield strength. The macroscopic behavior is driven by the TRIP effect, transformation of retained austenite to martensite, leading to discontinuous yielding and excellent formability. Also, smooth transition of hardness from ferrite to neighboring retained austenite and martensite is observed, resulting in beneficial effect on formability.
- DH steel exhibits a higher yield strength and moderate ductility. The higher initial yield strength is largely contributed from hard phase's martensite/bainite (55 %) that resist deformation. The interaction between hard martensite and soft ferrite leads to GNDs, which promote smooth, continuous yielding. Also, chemical heterogeneity due to Mn banding and gradient in hardness between soft/hard phases is observed.

CRediT authorship contribution statement

S. Janakiram: Writing – original draft, Investigation, Formal analysis, Data curation, Conceptualization. **Harita Seekala:** Investigation, Data curation. **Chavan Akash Naik:** Investigation, Data curation. **S. Chen:** Writing – review & editing, Formal analysis. **J.W.H. van Krevel:** Writing – review & editing, Formal analysis. **Leo A.I. Kestens:** Writing – review & editing, Formal analysis. **J. Gautam:** Writing – review & editing, Supervision, Formal analysis, Conceptualization. **P. Sudharshan Phani:** Writing – review & editing, Supervision, Formal analysis, Data curation, Conceptualization.

Data availability statement

The data that support the findings of this study are available from the corresponding author upon reasonable request.

Declaration of competing interest

The authors declare that they have no known competing financial interests or personal relationships that could have appeared to influence the work reported in this paper.

Acknowledgement

The authors would like to thank Tata Steel Research, Development and Technology (RD&T), IJmuiden, The Netherlands for supplying the materials and DST FIST and DST PURSE for the funding instrumentation facility (FESEM-EBSD). SJ, PSP and JG's contribution to this work was supported by University of Hyderabad IoE research project no UoH/IoE/RC3/21/040. CAN's contribution to this work was supported by IoE-IPDRF, University of Hyderabad.

Data availability

Data will be made available on request.

References

[1] Jiahao Chen, Junxiong Wang, Yanlin He, Yueshan Jiang, Li Lin, Xin Xu, Rendong Liu, Li Lin, Investigation on the interpretable machine-learning model for predicting mechanical properties of DH auto-steel plates, Mater. Today Commun. 46 (2025), https://doi.org/10.1016/j.mtcomm.2025.112674.

[2] S. Mirhosseini, E.S. Perdahcıoğlu, E.H. Atzema, A.H. van den Boogaard, Effect of temperature and heat generation on martensitic phase transformation in DH steels, Results Mater. 14 (2022), https://doi.org/10.1016/j.rinma.2022.100281.

[3] M. Soleimani, A. Kalhor, H. Mirzadeh, Transformation-Induced Plasticity (TRIP) in Advanced Steels: a Review, Elsevier B.V., 2020, https://doi.org/10.1016/j.msea.2020.140023.

[4] V. Alcántara, V.H. Peláez, V.A. Alza, V. Pelaez Chavez, TRIP steels: factors influencing their formation, mechanical properties and Microstructure-A review characterization of materials and heat treatments view project TRIP steels: factors influencing their formation, mechanical properties and Microstructure-A, IOSR J. Mech. Civ. Eng. e-ISSN. 19 (2022) 37–60, https://doi.org/10.9790/1684-1902023760.

[5] B.L. Ennis, E. Jimenez-Melero, E.H. Atzema, M. Krugla, M.A. Azeem, D. Rowley, D. Daisenberger, D.N. Hanlon, P.D. Lee, Metastable austenite driven work-hardening behaviour in a TRIP-Assisted dual phase steel, Int. J. Plast. 88 (2017) 126–139, https://doi.org/10.1016/j.ijplas.2016.10.005.

[6] Z. Hu, K. Wang, J. Guo, Microstructure and mechanical property of a novel hot dip galvanized dual phase steel with high ductility, J. Phys. Conf. Ser. 2368 (2022), https://doi.org/10.1088/1742-6596/2368/1/012021.

[7] A. Ebrahimian, S.S.G. Banadkouki, Materials science & engineering A effect of alloying element partitioning on ferrite hardening in a low alloy ferrite-martensite dual phase steel, Mater. Sci. Eng. 677 (2016) 281–289, https://doi.org/10.1016/j.msea.2016.09.073.

[8] E. Abbasi, W.M. Rainforth, Microstructural evolution during bainite transformation in a vanadium microalloyed TRIP-assisted steel, Mater. Sci. Eng. 651 (2016) 822–830, https://doi.org/10.1016/j.msea.2015.11.024.

[9] Y.G. Deng, H.S. Di, R.D.K. Misra, Microstructure and mechanical property relationship in a high strength high-Al low-Si hot-dip galvanized steel under quenching and partitioning process, J. Mater. Res. Technol. 9 (2020) 14401–14411, https://doi.org/10.1016/j.jmrt.2020.10.018.

[10] K.I. Sugimoto, N. Usui, M. Kobayashi, S.I. Hashimoto, Effects of volume fraction and stability of retained austenite on ductility of TRIP-aided dual-phase steels, ISIJ Int. 32 (1992) 1311–1318, https://doi.org/10.2355/isijinternational.32.1311.

[11] N. Zhao, M. Ding, L. Lin, Y. He, J. Wang, R. Zhang, Y. Zhang, R. Liu, L. Wang, L. Li, Insights into the relationship between γ/α transformation and strength-ductility of auto-steel with 980 MPa grade based on experiments and theoretical calculations, Vacuum 215 (2023) 112252, https://doi.org/10.1016/j.vacuum.2023.112252.

[12] C.C. Tasan, M. Diehl, D. Yan, M. Bechtold, F. Roters, L. Schemmann, C. Zheng, N. Peranio, D. Ponge, M. Koyama, K. Tsuzaki, D. Raabe, An overview of dual-phase steels: advances in microstructure-oriented processing and micromechanically guided design, Annu. Rev. Mater. Res. 45 (2015) 391–431, https://doi.org/10.1146/annurev-matsci-070214-021103.

[13] A. Khosravani, L. Morsdorf, C.C. Tasan, S.R. Kalidindi, Multiresolution mechanical characterization of hierarchical materials: spherical nanoindentation on martensitic Fe-Ni-C steels, Acta Mater. 153 (2018) 257–269, https://doi.org/10.1016/j.actamat.2018.04.063.

[14] Z. Xie, C. Song, W. Shen, H. Wang, Z. Sun, H. Yu, J. Cheng, First-principles study on the effect of Ce on segregation behavior of bcc-Fe grain boundaries in low-carbon low-alloy steel, J. Mater. Res. Technol. 36 (2025) 10474–10486, https://doi.org/10.1016/j.jmrt.2025.05.237.

[15] A. Abdulwahab, M, U. Shehu, Oyetunji, Effect of ferrite-martensite microstructural evolution on hardness and impact toughness behaviour of high martensite dual phase steel, Aust. J. Basic Appl. Sci. 1 (4) (2007) 407–414.

[16] A.H. Jahanara, Y. Mazaheri, M. Sheikhi, Correlation of ferrite and martensite micromechanical behavior with mechanical properties of ultrafine grained dual phase steels, Mater. Sci. Eng. 764 (2019) 138206, https://doi.org/10.1016/j.msea.2019.138206.

[17] M.D. Taylor, E. De Moor, J.G. Speer, D.K. Matlock, Effects of Constituent Hardness on Formability of Dual Phase Steels 2100281 (2021) 1–13, https://doi.org/10.1002/srin.202100281.

[18] S. Janakiram, P.S. Phani, G. Ummethala, S.K. Malladi, J. Gautam, L.A.I. Kestens, New insights on recovery and early recrystallization of ferrite-pearlite banded cold rolled high strength steels by high speed nanoindentation mapping, Scr. Mater. 194 (2021) 113676, https://doi.org/10.1016/j.scriptamat.2020.113676.

[19] C.A. Naik, B.K.S. Kumar, S. Harita, S. Roshan, S. Janakiram, P.S. Phani, J. P. Gautam, Assessment of structure-property relationships at the micrometer length scale in dual phase steels by electron microscopy and nanoindentation, Mater. Today Commun. 38 (2024) 107696, https://doi.org/10.1016/j.mtcomm.2023.107696.

[20] S. Janakiram, P.S. Phani, G. Ummethala, H.V. Jagdeesh, S.K. Malladi, J. Gautam, L. A.I. Kestens, Insights on early recovery kinetics in ferrite - pearlite cold rolled high strength sheet steels, Mater. Char. 193 (2022), https://doi.org/10.1016/j.matchar.2022.112332.

[21] E. Rossi, C. Tromas, Z. Liu, Y. Zou, J.M. Wheeler, Revealing new depths of information with indentation mapping of microstructures, MRS Bull. 50 (2025) 715–725, https://doi.org/10.1557/s43577-025-00919-6.

[22] J.M. Wheeler, Mechanical phase mapping of the Taza meteorite using correlated high-speed nanoindentation and EDX, J. Mater. Res. (2021), https://doi.org/10.1557/s43578-020-00056-7.

[23] Y. Chang, M. Lin, U. Hangen, S. Richter, C. Haase, W. Bleck, Revealing the relation between microstructural heterogeneities and local mechanical properties of complex-phase steel by correlative electron microscopy and nanoindentation characterization, Mater. Des. 203 (2021) 109620, https://doi.org/10.1016/j.matdes.2021.109620.

[24] Y. Chang, C. Haase, D. Szeliga, L. Madej, U. Hangen, M. Pietrzyk, W. Bleck, A compositional heterogeneity in multiphase steels : characterization and influence on local properties, Mater. Sci. Eng. 827 (2021) 142078, https://doi.org/10.1016/j.msea.2021.142078.

[25] A. El-Sherbiny, M.K. El-Fawkhry, A.Y. Shash, T. El-Hossany, Replacement of silicon by aluminum with the aid of vanadium for galvanized TRIP steel, J. Mater. Res. Technol. 9 (2020) 3578–3589, https://doi.org/10.1016/j.jmrt.2020.01.096.

[26] M. De Meyer, D. Vanderschueren, B.C. De Coomaim, The influence of the substitution of Si by AI on the properties of cold rolled C-Mn-Si TRIP steels, ISIJ Int. 39 (1999) 813–822, https://doi.org/10.2355/isijinternational.39.813.
[27] Amar K. De, John G. Speer, David K. Matlock, Color tint-etching for multiphase steels, Adv. Mater. Process. Process. 161 (2003) 27–30.
[28] R. De Melo, C. Lima, J.C. Spadotto, M. Isabel, R. Navarro, A.J. Clarke, K.D. Clarke, R. De Janeiro, A.S. Processing, F.I. Educational, Microstructural characterization of a 1200 MPa complex-phase steel, Mat. Res. 26 (2023), https://doi.org/10.1590/1980-5373-MR-2023-0015.
[29] I. Arganda-Carreras, V. Kaynig, C. Rueden, K.W. Eliceiri, J. Schindelin, A. Cardona, H.S. Seung, Trainable weka segmentation: a machine learning tool for microscopy pixel classification, Bioinformatics 33 (2017) 2424–2426, https://doi.org/10.1093/bioinformatics/btx180.
[30] E.A. Ariza-Echeverri, M. Masoumi, A.S. Nishikawa, D.H. Mesa, A.E. Marquez-Rossy, A.P. Tschiptschin, Development of a new generation of quench and partitioning steels: influence of processing parameters on texture, nanoindentation, and mechanical properties, Mater. Des. 186 (2020) 108329, https://doi.org/10.1016/j.matdes.2019.108329.
[31] P. Sudharshan Phani, W.C. Oliver, A critical assessment of the effect of indentation spacing on the measurement of hardness and modulus using instrumented indentation testing, Mater. Des. 164 (2019) 1–10, https://doi.org/10.1016/j.matdes.2018.107563.
[32] B. Vignesh, W.C. Oliver, G.S. Kumar, P.S. Phani, Critical assessment of high speed nanoindentation mapping technique and data deconvolution on thermal barrier coatings, Mater. Des. 181 (2019), https://doi.org/10.1016/j.matdes.2019.108084.
[33] F.G. Caballero, A. García-Junceda, C. Capdevila, C.G. De Andrés, Evolution of microstructural banding during the manufacturing process of dual phase steels, Mater. Trans. 47 (2006) 2269–2276, https://doi.org/10.2320/matertrans.47.2269.
[34] M. Calcagnotto, D. Ponge, E. Demir, D. Raabe, Orientation gradients and geometrically necessary dislocations in ultrafine grained dual-phase steels studied by 2D and 3D EBSD, Mater. Sci. Eng. 527 (2010) 2738–2746, https://doi.org/10.1016/j.msea.2010.01.004.
[35] S. Subedi, R. Pokharel, A.D. Rollett, Orientation gradients in relation to grain boundaries at varying strain level and spatial resolution, Mater. Sci. Eng. 638 (2015) 348–356, https://doi.org/10.1016/j.msea.2015.04.051.
[36] A. Ramazani, K. Mukherjee, A. Schwedt, P. Goravanchi, U. Prahl, W. Bleck, Quantification of the effect of transformation-induced geometrically necessary dislocations on the flow-curve modelling of dual-phase steels, Int. J. Plast. (2012), https://doi.org/10.1016/j.ijplas.2012.11.003.
[37] A. Khajesarvi, S.S.G. Banadkouki, S.A. Sajjadi, M.C. Somani, Abnormal trend of ferrite hardening in a Medium-Si ferrite-martensite dual phase steel, Metals 13 (2023), https://doi.org/10.3390/met13030542.
[38] S. Kim, C.G. Lee, T. Lee, C. Oh, Effect of Cu , Cr and Ni on mechanical properties of 0 . 15 wt .% C TRIP-aided cold rolled steels, Scr. Mater. 48 (2003) 539–544, https://doi.org/10.1016/S1359-6462(02)00477-3.
[39] I.B. Timokhina, P.D. Hodgson, S.P. Ringer, R.K. Zheng, E. V Pereloma, Precipitate characterisation of an advanced high-strength low-alloy, HSLA steel using atom probe tomography 56 (2007) 601–604, https://doi.org/10.1016/j.scriptamat.2006.12.018.
[40] Y. Sakuma, D.K. Matlock, G. Krauss, Intercritically annealed and isothermally transformed 0.15 Pct C steels containing 1.2 Pct Si-1.5 Pct Mn and 4 Pct Ni: part I. transformation, microstructure, and room-temperature mechanical properties, Metall. Mater. Trans. A. 23 (1992) 1221–1232, https://doi.org/10.1007/BF02665053.
[41] C. Song, Z. Xie, Z. Zhang, H. Wang, Z. Sun, Y. Yang, H. Yu, J. Cheng, Effect of Ce on the microstructure, mechanical properties and dislocation state in low-carbon low-alloy steels, Mater. Sci. Eng. 927 (2025) 148009, https://doi.org/10.1016/j.msea.2025.148009.
[42] R. Ranjan, H. Beladi, P.D. Hodgson, S.B. Singh, Yield point phenomenon in low-alloyed TRIP-aided steel: role of retained austenite, Mater. Sci. Technol. 39 (2023) 85–93, https://doi.org/10.1080/02670836.2022.2102281.